

A schistosomiasis model with an age-structure in human hosts ^{*}

Pei Zhang, Zhilan Feng and Fabio Milner
Department of Mathematics
Purdue University
West Lafayette, IN 47907

February 7, 2006

Abstract

We study a system of partial differential equations which models the disease transmission dynamics of schistosomiasis. Both the infection rate of human hosts and their treatment rate are assumed to be dependent on the age distribution of the human host population. The basic reproductive number is computed, and is shown to determine the stability of equilibria of the model. Numerical simulations show that stable periodic solutions exist for certain set of parameter values. Results of the deterministic model are compared with stochastic simulations. The effect of various age-targeted treatment strategies are discussed.

1 Introduction

The spread and persistence of schistosomiasis have always been among the more complex host-parasite processes to model mathematically, because of the several different forms that the parasites take while infecting two separate hosts (definitive human hosts and intermediate snail hosts) during their life cycle. For schistosome (and other helminth) parasites, the number of parasites infecting an individual host (i.e., the intensity of the infection) plays an important role in determining the outcome of an infection. Thus, transmission rates, pathogenicity, and development of host immunity are all typically assumed to depend upon intensity. These features preclude modeling the system through traditional (microparasite) *SIR* models. Macroparasite models are considered more appropriate as they take into consideration the distribution of parasites within human hosts (May and Anderson 1979). A number of mathematical models have been developed for schistosomiasis using a variety of approaches. The earliest models of schistosomiasis consider the population sizes of both humans and snails to be constant (Macdonald 1965, Nasell and Hirsch 1973). Several studies

^{*}Supported in part by NSF grant DMS-0314575.

in the last decades have addressed the dynamics of schistosomiasis and other helminth infection of humans (Anderson and May 1985, 1978, 1979, Anderson and Medley 1985, Anderson 1986, Diekmann and Kretzschmar 1991, Dobson 1988, Haderler 1984, Haderler and Dietz 1982, May and Anderson 1979, Woolhouse 1991). These models have made contributions to the understanding of the transmission dynamics of schistosomes. However, most existing models for schistosomiasis do not include explicitly the dynamics of the intermediate snail host.

Another important feature associated with schistosome parasites is that drug treatment of patients with schistosomiasis may select for drug-resistant parasites. Current control programs have focused on chemotherapy, which reduces morbidity by killing adult worms and diminishing egg deposition. Praziquantel (PZQ) remains the drug of choice for the treatment of schistosomiasis, but recent epidemiological evidence suggests the emergence of PZQ-resistant schistosomes [?]. The subject of schistosome resistance to chemotherapy has not been studied until a few years ago. Therefore, most mathematical models of schistosomiasis do not consider drug resistance of the parasites.

Also, just as many other diseases, schistosomiasis in humans is age-dependent (Chan *et al.* 1995). Epidemiological studies have shown that children of school age usually exhibit the highest prevalence of schistosome infections (Savioli *et al.* 1990, Warren *et al.* 1993) whereas adults exhibit some of the more serious consequences of infection (Homeida *et al.* 1988, WHO 1989). Various age-targeted treatments have been adopted in different populations and mathematical models have been used to assess the cost-effectiveness of disease control programs (Chan *et al.* 1995, Carabin *et al.* 2000). However, the models do not consider explicit snail population dynamics.

We have previously studied mathematical models incorporating mass chemotherapy in human hosts (see Feng *et al.* 2001) as well as infection-age-dependent cercariae release rate of snails and density-dependent birth rate of snails (see Feng *et al.* 2001, 2002). Neither of these two models include an age-structure in humans. Results in these studies lead to important conclusions: 1) If the parasite reproduction and virulence (parasite-related host death) are linked to resistance, then drug treatment may lead to the establishment of multiple parasite strains with different levels of resistance; 2) The mean parasite load of human hosts does not depend linearly on the transmission rate from snail to human as simpler models (simpler snail dynamics) predict, but rather on the square root of this transmission rate; 3) The density dependence considered in the model may produce a bifurcation at which the unique endemic equilibrium changes its stability and stable periodic solutions exist. In this paper, we develop a new mathematical model which includes both an age-structure of the human population and explicit snail population dynamics. The model is studied both analytically and numerically in terms of steady states and their stability as well as possible bifurcations. The model is then applied to the study of age-dependent disease control strategies.

2 The model formulation

Let N , P , and C denote the numbers of human hosts, adult parasites, and free-living cercariae, respectively. Assume that individuals are born uninfected. Based on the models in Anderson and May (1978) and Dobson (1988) we have developed an age-independent model

Table 1: Definition of parameters in Model (5).

Symbol	Definition
Λ_h	recruitment rate of human hosts
$\mu_h(a)$	per capita natural death rate of human hosts of age a
$\sigma(a)$	treatment rate of human hosts of age a
μ_p	per capita death rate of adult parasites
α	disease-induced death rate of human hosts by one cercaria
$\delta_p(a)$	$\mu_h(a) + \mu_p + \alpha + \sigma(a)$: “total” death rate of adult parasites
$\beta(a)$	instantaneous rate of infection of human hosts of age a by one cercaria
k	clumping parameter of the parasite distribution within humans
$b(S, I)$	birth function of uninfected snails
$b_1(S, I)$	Λ_s : Constant birth rate of snails
$b_2(S, I)$	$c_1 S / (c_2 + S + I)$: density-dependent birth function of snails
c_1, c_2	saturation and scaling constant respectively
μ_s	per capita natural death rate of snails
δ_s	disease-induced death rate of infection of snails by parasites
γ	per capita rate of effective egg-production (or miracidia) of adult parasites
ρ	per capita infection rate of snails by miracidia
ξ	$\rho\gamma$: per capita infection rate of snails by adult parasites
$r(\tau)$	rate at which infected snails of infection-age τ release cercariae

(see Feng *et al.* 2001) in which the equation for the total number of adult parasites, P , has the form:

$$\frac{dP}{dt} = \beta CN - (\mu_h + \mu_p + \alpha + \sigma)P - \alpha \left(\frac{1+k}{k} \right) \frac{P^2}{N} \quad (1)$$

where β is the instantaneous rate of infection of human hosts by one cercaria, μ_h is the per capita natural death rate of human hosts, μ_p is the per capita death rate of adult parasites, α is the disease-induced death rate of humans *per parasite*; σ is the treatment rate of human hosts, k is the clumping parameter of the binomial distribution of parasites. All parameters and variables together with their definitions are listed in Table 1.

Let $n(t, a)$, $p(t, a)$ denote the density functions of human hosts of age a at time t and parasites within human hosts of age a , respectively. We remark that a denotes the age of humans (not the parasites). We can use the same approach to derive the equations for $n(t, a)$ and $p(t, a)$, and get:

$$\begin{aligned} \frac{\partial}{\partial t} n(t, a) + \frac{\partial}{\partial a} n(t, a) &= -\mu_h(a)n(t, a) - \alpha p(t, a), \\ \frac{\partial}{\partial t} p(t, a) + \frac{\partial}{\partial a} p(t, a) &= \beta(a)Cn(t, a) - d(a)p(t, a) - \alpha \frac{1+k}{k} \frac{P(t)}{N(t)} p(t, a), \end{aligned} \quad (2)$$

where

$$\delta_p(a) = \mu_h(a) + \mu_p + \alpha + \sigma(a). \quad (3)$$

The boundary conditions are $n(t, 0) = \Lambda_h$ (birth rate of human hosts), $p(t, 0) = 0$ (humans are born uninfected), and initial conditions are $n(0, a) = n_0(a)$, $p(0, a) = p_0(a)$ for some given functions n_0 and p_0 . $P(t)$ is the total number of adult parasites at time t given by $P(t) = \int_0^\infty p(t, a) da$, and $N(t)$ is the total number of humans at time t given by $N(t) = \int_0^\infty n(t, a) da$. P/N represents the mean parasite load, and C is determined by the number of infected snails whose equation is given later in the system for snails.

We should remark that the birth rate of human hosts is taken to be constant in order to make the analysis simpler and to allow for some formulas to become explicit rather than implicit. In human demography the birth rate is usually modeled linearly as

$$n(t, 0) = \int_0^\infty f(a)n(t, a) da,$$

where $f(a)$ is the age-specific fertility at age a . If we assume the human population is at steady state, then the birth rate is obviously constant and it is under this assumption that we shall work.

For the snail dynamics, we can use similar equations to those introduced in Feng *et al.* (2002) taking into consideration realistic features including an infection-age-dependent cercariae release rate of infected snails and a density-dependent snail birth rate due to the infertility of infected snails:

$$\begin{aligned} \frac{d}{dt}S &= b(S, I) - \mu_s S - \rho M S, \\ \frac{\partial}{\partial t}x(t, \tau) + \frac{\partial}{\partial \tau}x(t, \tau) &= -(\mu_s + \delta)x(t, \tau), \\ x(t, 0) &= \rho M S, \quad x(0, \tau) = x_0(\tau), \\ C(t) &= \int_0^\infty r(\tau)x(t, \tau)d\tau. \end{aligned} \quad (4)$$

S denotes the number of uninfected snails. I denotes the total number of infected snails given by $I(t) = \int_0^\infty x(t, \tau)d\tau$. Here, τ denotes the time since infection, i.e., infection-age, and $x(t, \tau)$ denotes the infection-age density of snails at time t . $M = \gamma P$ is the number of free-living miracidia (since miracidia die quickly if they cannot find a snail to infect, the total number of miracidia at time t is assumed to be proportional to the number of adult parasites) and γ is the per capita effective egg-production rate of adult parasites. Other parameters are: $b(S, I)$ is the birth function of uninfected snails, μ_s is the per capita natural death rate of snails, δ is the disease-induced death rate of snails, ρ is the per capita rate of infection of snails, and $r(\tau)$ denotes the rate at which infected snails of infection-age τ release cercariae. Two forms of the birth function $b(S, I)$ will be considered, as done in Feng *et al.* (2002). One will be constant and the other a Michaelis-Menten type function, $b(S, I) = c_1 S / (c_2 + S + I)$, which assumes that infected snails do not reproduce and that the per capita birth rate is density-dependent; c_1 and c_2 are, respectively, the scaling and saturation constants.

The combination of (2) and (4) leads to the following integro-differential initial-boundary value problem that governs the disease dynamics:

$$\left\{ \begin{array}{l} \frac{\partial}{\partial t} n(t, a) + \frac{\partial}{\partial a} n(t, a) = -\mu_h(a)n(t, a) - \alpha p(t, a), \\ \frac{\partial}{\partial t} p(t, a) + \frac{\partial}{\partial a} p(t, a) = \beta(a)Cn(t, a) - \delta_p(a)p(t, a) - \alpha \frac{1+k}{k} \frac{P(t)}{N(t)} p(t, a), \\ \frac{d}{dt} S(t) = b(S, I) - \mu_s S(t) - \rho\gamma S(t) \int_0^\infty p(t, a) da, \\ \frac{\partial}{\partial t} x(t, \tau) + \frac{\partial}{\partial \tau} x(t, \tau) = -(\mu_s + \delta_s)x(t, \tau), \\ P(t) = \int_0^\infty p(t, a) da, \quad C(t) = \int_0^\infty r(\tau)x(t, \tau) d\tau, \quad I(t) = \int_0^\infty x(t, \tau) d\tau, \\ n(t, 0) = \Lambda_h, \quad p(t, 0) = 0, \quad x(t, 0) = \rho\gamma S(t) \int_0^\infty p(t, a) da, \\ n(0, a) = n_0(a), \quad p(0, a) = p_0(a), \quad S(0) = S_0, \quad I(0) = I_0, \quad x(0, \tau) = x_0(\tau). \end{array} \right. \quad (5)$$

The large number of parameters involved in system (4) can be reduced as several of the parameters can be lumped together. However, we choose to show these parameters explicitly since they are more readily related to field data. We plan to use techniques based on Latin hypercube sampling (see Sanchez and Blower 1997) to identify quantitatively the most influential parameter(s) affecting the magnitude of threshold conditions through uncertainty and sensitivity analysis.

3 Analysis

In this section we compute the reproductive number of the disease, \mathcal{R} , and show that it determines the existence and stability of non-trivial equilibrium points. For mathematical convenience we consider a different formulation of the system (5) as shown below.

3.1 Reformulation of system (5)

For ease of notation we introduce a new variable B :

$$B(t) = \rho\gamma S(t) \int_0^\infty p(t, a) da = \rho\gamma S(t) P(t).$$

Solving the x -equation along the characteristic lines we get

$$x(t, \tau) = \begin{cases} e^{-(\mu_s + \delta_s)\tau} B(t - \tau), & t \geq \tau, \\ e^{-(\mu_s + \delta_s)\tau} x_0(\tau - t), & t < \tau. \end{cases}$$

Then $I(t)$ and $C(t)$ can be expressed in terms of $B(t)$:

$$\begin{aligned} C(t) &= \int_0^t r(\tau)e^{-(\mu_s+\delta_s)\tau}B(t-\tau)d\tau + F_1(t), \\ I(t) &= \int_0^t e^{-(\mu_s+\delta_s)\tau}B(t-\tau)d\tau + F_2(t), \end{aligned} \quad (6)$$

where

$$\begin{aligned} F_1(t) &= \int_t^\infty r(\tau)e^{-(\mu_s+\delta_s)\tau}x_0(\tau-t)d\tau, \\ F_2(t) &= \int_t^\infty e^{-(\mu_s+\delta_s)\tau}x_0(\tau-t)d\tau. \end{aligned}$$

Using this notation we can rewrite system (5) as

$$\left\{ \begin{aligned} \frac{\partial}{\partial t}n(t, a) + \frac{\partial}{\partial a}n(t, a) &= -\mu_h(a)n(t, a) - \alpha p(t, a), \\ \frac{\partial}{\partial t}p(t, a) + \frac{\partial}{\partial a}p(t, a) &= \beta(a)n(t, a) \int_0^t r(\tau)e^{-(\mu_s+\delta_s)\tau}B(t-\tau)d\tau \\ &\quad - \delta_p(a)p(t, a) - \alpha k_0 \frac{P(t)}{N(t)}p(t, a) + \beta(a)n(t, a)F_1(t), \\ \frac{d}{dt}S(t) &= b(S, I) - \mu_s S(t) - B(t), \\ B(t) &= \xi P(t)S(t), \end{aligned} \right. \quad (7)$$

where

$$\xi = \rho\gamma, \quad k_0 = \frac{k+1}{k}.$$

The existence and uniqueness of solutions for system (7) can be shown using standard methods. Notice that $F_1(t) \rightarrow 0$ as $t \rightarrow \infty$. The limiting system of (7) is:

$$\left\{ \begin{aligned} \frac{\partial}{\partial t}n(t, a) + \frac{\partial}{\partial a}n(t, a) &= -\mu_h(a)n(t, a) - \alpha p(t, a), \\ \frac{\partial}{\partial t}p(t, a) + \frac{\partial}{\partial a}p(t, a) &= \beta(a)n(t, a)(K * B)(t) - \delta_p(a)p(t, a) - \alpha k_0 \frac{P(t)}{N(t)}p(t, a), \\ \frac{d}{dt}S(t) &= b(S, I) - \mu_s S(t) - B(t), \\ B(t) &= \xi P(t)S(t), \end{aligned} \right. \quad (8)$$

where

$$K(\tau) = r(\tau)e^{-(\mu_s+\delta_s)\tau}$$

And

$$(K * B)(t) = \int_0^\infty K(\tau)B(t-\tau)d\tau.$$

In the rest of this section we consider the limiting system (8).

3.2 The reproductive number of the parasite

As done in Feng *et al.* (2002) we consider two forms of the snail birth function $b(S, I)$.

Case 1: $b_1(S, I) = \Lambda_s$ (constant birth rate).

System (8) always has the parasite-free equilibrium

$$E_0 = (n_0(a), p_0(a), S_0, B_0) = (\Lambda_h \pi(a), 0, \Lambda_s / \mu_s, 0).$$

As in most epidemiology models, the stability of E_0 is dependent on the basic reproductive number of the parasites, or the reproductive number of the parasites if the host population is under some control/prevention program, as is the case in the models we consider. We define the reproductive number of the parasites as

$$\mathcal{R} = \int_0^\infty \beta(w) \mathcal{K} \Lambda_h \pi(w) \int_0^\infty \xi \frac{\Lambda_s}{\mu_s} e^{-\int_w^{w+u} \delta_p(\theta) d\theta} du dw, \quad (9)$$

where

$$\pi(a) = e^{-\int_0^a \mu_h(\theta) d\theta}$$

represents the survival probability of a person up to age a , $\delta_p(\theta) = \mu_h(\theta) + \mu_p + \alpha + \sigma(\theta)$ is the total death rate of the parasites within a human host of age θ , and

$$\mathcal{K} = \int_0^\infty r(\tau) e^{-(\mu_s + \delta_s)\tau} d\tau = \int_0^\infty K(\tau) d\tau$$

represents the total number of cercariae released by an infected snail during its life of infection. For convenience of interpretation, we consider the secondary number of infected snails (instead of parasites) produced by a typical infected snail during its entire period of infection. The quantity

$$\beta(w) \mathcal{K} \Lambda_h \pi(w)$$

represents the average number of human hosts of age w becoming infected by one infected snail during its entire period of infection. $e^{-\int_w^{w+u} \delta_p(\theta) d\theta}$ is the survival probability of a parasite in a human host of age $w + u$ who was infected at age w , and the average number of snails the parasite (u time units after the host was infected, or parasite of age u) is capable of infecting is $\xi \Lambda_s / \mu_s e^{-\int_w^{w+u} \delta_p(\theta) d\theta}$. Thus, the total number of snails infected by a typical such parasite during its entire life time is

$$\int_0^\infty \xi \frac{\Lambda_s}{\mu_s} e^{-\int_w^{w+u} \delta_p(\theta) d\theta} du.$$

It follows that the number of secondary snail infections due to a human host of age w is

$$\beta(w) \mathcal{K} \Lambda_h \pi(w) \int_0^\infty \xi \frac{\Lambda_s}{\mu_s} e^{-\int_w^{w+u} \delta_p(\theta) d\theta} du. \quad (10)$$

Integrating over all ages $w \in [0, \infty)$ we obtain the overall average number of secondary snail infections, which is the number \mathcal{R} given in (9).

Case 2: $b_2(S, I) = c_1 S / (c_2 + S + I)$ (density-dependent birth rate).

Here c_1 and c_2 are the scaling and saturation constants, respectively. In this case the reproductive number is

$$\mathcal{R}' = \mathcal{R}'_{MS} \mathcal{R}'_{SM} \quad (11)$$

where

$$\mathcal{R}'_{SM} = \left(\int_0^\infty \Lambda_h \pi(a) da \right) \left(\int_0^\infty \beta r(\tau) e^{-(\mu_s + \delta_s)\tau} d\tau \right)$$

represents the contribution from the snail-to-man transmission and

$$\mathcal{R}'_{MS} = \xi \bar{S} \int_0^\infty \pi(a) \pi_1(a) e^{-(\mu_p + \alpha)a} da$$

represents the contribution from the man-to-snail transmission with

$$\bar{S} = \frac{c_1}{\mu_s} - c_2 > 0, \quad \pi_1(a) = e^{-\int_0^\infty \delta_p(s) ds}. \quad (12)$$

being the snail carrying capacity of the environment in the absence of parasites.

3.3 Steady states and their stability for the case of $b_1(S, I)$

In this Section we consider the case of constant snail recruitment rate, i.e., $b_1(S, I) = \Lambda_s$. As in most epidemiology models, the reproductive number \mathcal{R} calculated above provides threshold conditions that determine whether the parasites will go extinct or will persist in the host population. The next result shows that parasite population will go extinct if \mathcal{R} is below 1.

Theorem 1 *The disease-free steady state E_0 of the system (8) is locally asymptotically stable if $\mathcal{R} < 1$ and unstable if $\mathcal{R} > 1$.*

Proof: Linearize the system (8) about E_0 and consider exponential solutions of the form

$$p(t, a) = p_1(a) e^{\lambda t} + o(e^{2\lambda t}), \quad B(t) = B_1 e^{\lambda t} + o(e^{2\lambda t}),$$

as $t \rightarrow \infty$. Then the linear parts of the p and B equations are

$$\begin{aligned} \frac{dp_1(a)}{da} &= \beta(a) \Lambda_h \pi(a) B_1 \hat{K}(\lambda) - (\delta_p(a) + \lambda) p_1(a), \\ B_1 &= \xi \frac{\Lambda_s}{\mu_s} \int_0^\infty p_1(a) da, \end{aligned} \quad (13)$$

where $\hat{f}(\lambda)$ denotes the Laplace transform of $f(\tau)$, i.e.,

$$\hat{f}(\lambda) = \int_0^\infty e^{-\lambda\tau} f(\tau) d\tau.$$

Solving the p_1 equation in (13) and noticing that $p_1(0) = 0$ we get

$$p_1(a) = \int_0^a \beta(u) \hat{K}(\lambda) B_1 \Lambda_h \pi(u) e^{-\int_u^a (d(s)+\lambda) ds} du.$$

Substituting the above expression for $p_1(a)$ in the B_1 equation in (13) we have

$$B_1 = \xi \frac{\Lambda_s}{\mu_s} \int_0^\infty \int_0^a \beta(u) \hat{K}(\lambda) B_1 \Lambda_h \pi(u) e^{-\int_u^a (d(s)+\lambda) ds} du da \quad (14)$$

By changing the order of integration, introducing $\tau = a - u$, and dividing both sides by B_1 (since $B_1 \neq 0$) in (14) we get the characteristic equation

$$1 = \int_0^\infty \int_0^\infty \beta(u) \hat{K}(\lambda) \Lambda_h \pi(u) \xi \frac{\Lambda_s}{\mu_s} e^{-\int_u^{u+\tau} (d(s)+\lambda) ds} d\tau du. \quad (15)$$

Let $G(\lambda)$ denote the right hand side of (15). Notice that $\int_u^{u+\tau} d(s) ds = \int_0^\tau d(\theta+u) d\theta$. Then, at $\lambda = 0$,

$$G(0) = \int_0^\infty \beta(u) \mathcal{K} \Lambda_h \pi(u) \int_0^\infty \xi \frac{\Lambda_s}{\mu_s} e^{-\int_0^\tau d(\theta+u) d\theta} d\tau du = \mathcal{R}. \quad (16)$$

It is easy to see $G'(\lambda) < 0$, $\lim_{\lambda \rightarrow \infty} G(\lambda) = 0$, $\lim_{\lambda \rightarrow -\infty} G(\lambda) = \infty$. It follows that the equation $G(\lambda) = 1$ has a unique root $\lambda^* < 0$ if $G(0) < 1$ (or $\mathcal{R} < 1$), and $\lambda^* > 0$ if $G(0) > 1$ (or $\mathcal{R} > 1$). Let $\lambda = x + iy$ be an arbitrary complex solution to $G(\lambda) = 1$. Then

$$1 = G(\lambda) = |G(x + iy)| \leq G(x),$$

which implies that $\lambda^* > x$. It follows that the parasite-free steady state is l.a.s. if $\mathcal{R} < 1$, and unstable if $\mathcal{R} > 1$.

Our next result shows that an endemic steady state exists when $\mathcal{R} > 1$.

Theorem 2 *If $\mathcal{R} > 1$ and the per capita disease-induced mortality rate of humans α is sufficiently small, system (8) has an unique endemic steady state and it is locally asymptotically stable.*

Proof: Recall that α represents the disease-induced human death rate by a single parasite. Thus, α is very small. For the analytic proof of this result we let $\alpha = 0$. For the case of $\alpha > 0$ the result seems to also be confirmed through numerical simulations.

Let $E^* = (n^*(a), p^*(a), S^*, B^*)$ denote the endemic steady state with positive components, and let $N^* = \int_0^\infty n^*(a) da$ and $P^* = \int_0^\infty p^*(a) da$. We first prove the result for the case when $\alpha = 0$. The Implicit Function Theorem can be then applied to extend the result to the case when $\alpha > 0$ is small enough.

Let $\alpha = 0$. Then $n^*(a) = \Lambda_h \pi(a)$, and E^* satisfies

$$\begin{cases} \frac{d}{da} p^*(a) = \beta(a) \Lambda_h \pi(a) \mathcal{K} B^* - \delta_p(a) p^*(a), \\ 0 = \Lambda_s - \mu_s S^* - B^*, \\ B^* = \xi P^* S^*. \end{cases} \quad (17)$$

Solving for $p^*(a)$ we get

$$p^*(a) = \int_0^a \beta(u) \Lambda_h \pi(u) B^* \mathcal{K} e^{-\int_u^a \delta_p(s) ds} du. \quad (18)$$

Substituting this into the B^* equation in (17) we get

$$B^* = \xi S^* \int_0^\infty \int_0^a \beta(u) \Lambda_h \pi(u) B^* \mathcal{K} e^{-\int_u^a \delta_p(s) ds} du da \quad (19)$$

By changing the order of integration, introducing $\tau = a - u$, and dividing both sides by B^* we get the following equation for S^* :

$$1 = \int_0^\infty \beta(u) \mathcal{K} \Lambda_h \pi(u) \int_0^\infty \xi S^* e^{-\int_u^{u+\tau} \delta_p(s) ds} d\tau du =: H(S^*). \quad (20)$$

For E^* to be biologically feasible, we need to require $S^* \in (0, \Lambda_s / \mu_s)$. Since $H(0) = 0$ and $H(\Lambda_s / \mu_s) = \mathcal{R} > 1$, the monotonicity of $H(S^*)$ implies that $H(S^*) = 1$ has a unique root S^* in $(0, \Lambda_s / \mu_s)$. We can then get $B^* = \Lambda_s - \mu_s S^*$ using the second equation in (17) and then $p^*(a)$ using equation (18). Thus, we have a unique endemic steady state E^* when $\mathcal{R} > 1$.

We proceed to show the stability of E^* . Since $\alpha = 0$, system (8) becomes

$$\begin{aligned} \frac{\partial}{\partial t} n(t, a) + \frac{\partial}{\partial a} n(t, a) &= -\mu_h(a) n(t, a), \\ \frac{\partial}{\partial t} p(t, a) + \frac{\partial}{\partial a} p(t, a) &= \beta(a) n(t, a) (K * B)(t) - \delta_p(a) p(t, a), \\ \frac{d}{dt} S(t) &= b(S, I) - \mu_s S(t) - B(t), \\ B(t) &= \xi P(t) S(t). \end{aligned} \quad (21)$$

Note that at E^*

$$n^*(a) = \Lambda_h \pi(a), \quad P^* = \frac{\mu_s}{\xi} (\tilde{\mathcal{R}}_0 - 1), \quad S^* = \frac{1}{\tilde{\mathcal{R}}_0} \frac{\Lambda_s}{\mu_s}. \quad (22)$$

where the $\tilde{\mathcal{R}}_0 = \mathcal{R}$ evaluated at $\alpha = 0$.

Solving the n -equation in (21) along the characteristic lines

$$n(t, a) = \begin{cases} \Lambda_h \pi(a), & t > a, \\ n_0(a) \frac{\pi(a)}{\pi(a-t)}, & t \leq a, \end{cases} \quad (23)$$

and substituting this into the p -equation in (21) we get

$$p(t, a) = \begin{cases} \Lambda_h (K * B)(t) \int_0^a \beta(w) \pi(w) e^{-\int_w^a \delta_p(s) ds} dw, & t > a, \\ q(t, a), & t \leq a, \end{cases} \quad (24)$$

where

$$q(t, a) = n_0(a)(K * B)(t) \frac{\pi(a)}{\pi(a-t)} \int_0^a \beta(w) \pi_1(w) e^{-\mu_p w} dw + \pi(a) \pi_1(a) e^{-\mu_p a} p_0(a-t).$$

Then

$$P(t) = \tilde{\mathcal{R}}_0 \frac{1}{\xi \mathcal{K}} \frac{\mu_s}{\Lambda_s} (K * B)(t) + Q(t)$$

where $Q(t) = \int_t^\infty q(t, a) da$. Noticing that $Q(t) \rightarrow 0$ as $t \rightarrow \infty$, we have the following limiting system for $P(t)$ and $S(t)$ (see (21))

$$\begin{cases} P(t) = \tilde{\mathcal{R}}_0 \frac{1}{\mathcal{K}} \frac{\mu_s}{\Lambda_s} (K * (PS))(t), \\ \frac{d}{dt} S(t) = \Lambda_s - \mu_s S(t) - \xi P(t) S(t). \end{cases} \quad (25)$$

The linearization of (25) at (P^*, S^*) (P^* and S^* are given in (17)) yields the following characteristic equation

$$\lambda + \mu_s \tilde{\mathcal{R}}_0 + \mu_s \frac{\hat{K}(\lambda)}{\mathcal{K}} \frac{1}{1 - \frac{\hat{K}(\lambda)}{\mathcal{K}}} (\tilde{\mathcal{R}}_0 - 1) = 0 \quad (26)$$

where λ is an eigenvalue and $\hat{f}(\lambda)$ denotes the Laplace transform of f . We need to show that (26) does not have a root with nonnegative real part when $\tilde{\mathcal{R}} > 1$. Let $\lambda = x + yi$ be a root of (26) with x and y real, i.e.

$$x + yi + \mu_s \tilde{\mathcal{R}}_0 + \mu_s \frac{\hat{K}(x + yi)}{\mathcal{K} - \hat{K}(x + yi)} (\tilde{\mathcal{R}}_0 - 1) = 0. \quad (27)$$

Introducing the notation

$$\begin{aligned} \mathcal{K}_c &= \int_0^\infty K(t) e^{-xt} \cos yt dt, \\ \mathcal{K}_s &= \int_0^\infty K(t) e^{-xt} \sin yt dt. \end{aligned}$$

Noticing that

$$\begin{aligned} \frac{\hat{K}(x + yi)}{\mathcal{K} - \hat{K}(x + yi)} &= \frac{\int_0^\infty K(t) e^{-xt - iyt} dt}{\int_0^\infty K(t) dt - \int_0^\infty K(t) e^{-xt - iyt} dt} \\ &= \frac{\int_0^\infty K(t) dt}{\int_0^\infty K(t) dt - \int_0^\infty K(t) e^{-xt - iyt} dt} - 1 \\ &= \frac{\int_0^\infty K(t) dt}{\int_0^\infty K(t) (1 - e^{-xt} \cos yt) dt + i \int_0^\infty K(t) e^{-xt} \sin yt dt} - 1 \\ &= \frac{\mathcal{K}(\mathcal{K} - \mathcal{K}_c)}{[\mathcal{K} - \mathcal{K}_c]^2 + (\mathcal{K}_s)^2} - 1 + \left(-\frac{\mathcal{K}\mathcal{K}_s}{[\mathcal{K} - \mathcal{K}_c]^2 + (\mathcal{K}_s)^2} \right) i \end{aligned}$$

And, separating the real and imaginary parts of the left hand side of (27), we get

$$\begin{cases} x + \mu_s \tilde{\mathcal{R}}_0 + \mu_s \left(\frac{\mathcal{K}(\mathcal{K} - \mathcal{K}_c)}{[\mathcal{K} - \mathcal{K}_c]^2 + (\mathcal{K}_s)^2} - 1 \right) (\tilde{\mathcal{R}}_0 - 1) = 0, \\ y - \mu_s \frac{\mathcal{K}\mathcal{K}_s}{[\mathcal{K} - \mathcal{K}_c]^2 + (\mathcal{K}_s)^2} (\tilde{\mathcal{R}}_0 - 1) = 0. \end{cases} \quad (28)$$

From the second equation in (28) we have

$$\frac{\mathcal{K}}{[\mathcal{K} - \mathcal{K}_c]^2 + (\mathcal{K}_s)^2} = \frac{y}{\mu_s} \frac{1}{\tilde{\mathcal{R}}_0 - 1} \frac{1}{\mathcal{K}_s},$$

and substituting this into the first equation in (28) we have

$$x + \mu_s \tilde{\mathcal{R}}_0 + \mu_s \left((\mathcal{K} - \mathcal{K}_c) \frac{y}{\mu_s} \frac{1}{\tilde{\mathcal{R}}_0 - 1} \frac{1}{\mathcal{K}_s} - 1 \right) (\tilde{\mathcal{R}}_0 - 1) = 0,$$

which simplifies to

$$x + y \frac{\mathcal{K} - \mathcal{K}_c}{\mathcal{K}_s} + \mu_s = 0. \quad (29)$$

However, from

$$\frac{\mathcal{K}}{[\mathcal{K} - \mathcal{K}_c]^2 + \mathcal{K}_s^2} = \frac{y}{\mu_s} \frac{1}{\tilde{\mathcal{R}}_0 - 1} \frac{1}{\mathcal{K}_s} = \frac{y}{\mathcal{K}_s} \frac{1}{\tilde{\mathcal{R}}_0 - 1} \frac{1}{\mu_s}$$

we have $\frac{y}{\mathcal{K}_s} > 0$, which yields

$$x = -y \frac{\mathcal{K} - \mathcal{K}_c}{\mathcal{K}_s} - \mu_s < 0$$

as $\mathcal{K}_c < \mathcal{K}$. Hence all eigenvalues have negative real part. It follows that $P(t) \rightarrow P^*$ and $S(t) \rightarrow S^*$ as $t \rightarrow \infty$. Consequently, $p(t, a) \rightarrow p^*(a)$ as $t \rightarrow \infty$ (see (18)). From (23) it is clear that $n(t, a) \rightarrow n^*(a)$ as $t \rightarrow \infty$. Therefore, E^* is l.a.s. if $\alpha = 0$. As indicated earlier, this result is valid for $\alpha > 0$ sufficiently small. For $\alpha > 0$ this seems to be the case in general as indicated by numerical simulations (see Figure 1). Figure 1 shows that the number of parasites $P(t)$ asymptotically goes to zero if $\mathcal{R} < 1$ (see Figures 1(a)) and it stabilizes at a positive level if $\mathcal{R} > 1$ (see Figures 1(b) and (c)). The proof of Theorem 2 is thus complete.

The following result shows that when $\mathcal{R} < 1$ the parasite-free steady state is actually globally asymptotically stable.

Theorem 3 *If $\mathcal{R} < 1$, E_0 is a global attractor, i.e.*

$$\lim_{t \rightarrow \infty} (n(t, a), p(t, a), S(t)) = \left(\Lambda_h \pi(a), 0, \frac{\Lambda_s}{\mu_s} \right)$$

for all positive solutions of system (8).

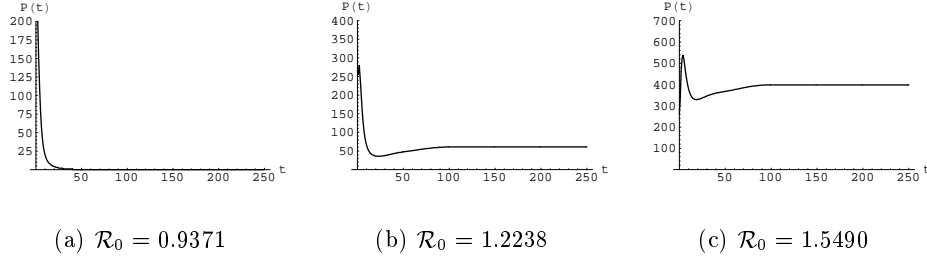


Figure 1: Plots of the number of adult parasites $P(t)$ vs. time. In (a) $\mathcal{R} < 1$, and the parasite population dies out. In (b) and (c) $\mathcal{R} > 1$, and the parasite population stabilizes at a positive level which increases with \mathcal{R} .

Proof: Let

$$S^\infty = \limsup_{t \rightarrow \infty} S(t), \quad P^\infty = \limsup_{t \rightarrow \infty} P(t), \quad P_\infty = \liminf_{t \rightarrow \infty} P(t).$$

Using Corollary 2.4 in [16] there is a sequence $t_n \rightarrow \infty$ such that $\frac{dS(t_n)}{dt} \rightarrow 0$ and $S(t_n) \rightarrow S^\infty$ as $n \rightarrow \infty$. Using this sequence and the S equation in (25) we get

$$0 \leq \Lambda_s - \mu_s S^\infty - \xi P_\infty S^\infty.$$

Since $P_\infty \geq 0$, the above inequality implies

$$S^\infty \leq \frac{\Lambda_s}{\mu_s + \xi P_\infty} \leq \frac{\Lambda_s}{\mu_s}.$$

Then from the P -equation in (25) we have

$$P^\infty \leq P^\infty S^\infty \tilde{\mathcal{R}} \frac{\mu_s}{\Lambda_s} \leq P^\infty \tilde{\mathcal{R}}. \quad (30)$$

Since $\tilde{\mathcal{R}} < 1$, the above inequality implies that $P^\infty = 0$, i.e., $\lim_{t \rightarrow \infty} P(t) = 0$. Using this and the S -equation in (25) we get $\lim_{t \rightarrow \infty} S(t) = \Lambda_s / \mu_s$. Noticing that $\lim_{t \rightarrow \infty} B(t) = \lim_{t \rightarrow \infty} \xi P(t) S(t) = 0$ we have from (24) that $\lim_{t \rightarrow \infty} p(t, a) = 0$ for all a . It is obvious from (23) that $\lim_{t \rightarrow \infty} n(t, a) = \Lambda_h \pi(a)$ for all a .

This completes the proof of Theorem 3.

3.4 Steady states and stability for the case of $b_2(S, I)$

In this case the reproductive number \mathcal{R}' is give by (11). The parasite-free steady state is

$$E'_0 = (\Lambda_h \pi(a), 0, \bar{S}),$$

where \bar{S} is given by (12). Similarly to the case of $b_1(S, I)$ we have the following global stability of E'_0 .

Theorem 4 E'_0 is a global attractor if $\mathcal{R}' < 1$ and it is unstable if $\mathcal{R}' > 1$.

Proof: The proof is largely the same as that for the case of $b_1(S, I)$ (see Theorems 1 and 3).

The existence and the stability of the endemic steady state are more difficult to prove than the case of constant birth rate of snails. In fact, the following result show that the endemic steady state is not always stable in the case of density dependent birth rate of snails, $b_2(S, I)$.

Theorem 5 (a) *System (8) has a unique endemic equilibrium E^\diamond if $\mathcal{R}' > 1$; (b) A Hopf bifurcation occurs at a critical value of the parameter $c_1 = \bar{c}_1$ such that E^\diamond is l.a.s. if $c_1 < \bar{c}_1$ and unstable if $c_1 > \bar{c}_1$, in which case stable periodic solutions exist.*

Proof: (a) Again we give an analytical proof of the existence only for the case when $\alpha = 0$. Let $E^\diamond = (n^\diamond(a), p^\diamond(a), S^\diamond, I^\diamond)$ denote the endemic steady state and let $P^\diamond = \int_0^\infty p^\diamond(a) da$. Then $P^\diamond > 0$, $n^\diamond(a) = \Lambda_h \pi(a)$, and $p^\diamond(a), S^\diamond, I^\diamond$ satisfy the equations (see (21) and (6))

$$\begin{cases} \frac{d}{da} p^\diamond(a) = \beta(a) \Lambda_h \pi(a) \mathcal{K} \xi P^\diamond S^\diamond - \delta_p(a) p^\diamond(a), \\ 0 = \frac{c_1 S^\diamond}{c_2 + S^\diamond + I^\diamond} - \mu_s S^\diamond - \xi P^\diamond S^\diamond, \\ I^\diamond = \frac{\xi P^\diamond S^\diamond}{\mu_s + \delta_s}. \end{cases} \quad (31)$$

Integrating the p^\diamond -equation and dividing by P^\diamond ($P^\diamond > 0$) we get

$$S^\diamond = \frac{1}{\tilde{\mathcal{R}}'} \bar{S} \quad (32)$$

where $\tilde{\mathcal{R}}' = \mathcal{R}'$ evaluated at $\alpha = 0$ and $\bar{S} > 0$ is given in (12). Using (32) and the last two equations in (31) we get

$$\frac{c_1}{c_2 + \frac{1}{\tilde{\mathcal{R}}'} \frac{\xi}{\mu_s + \delta_s} \bar{S} P^\diamond + \frac{1}{\tilde{\mathcal{R}}'} \bar{S}} = \mu_s + \xi P^\diamond,$$

which can be written as

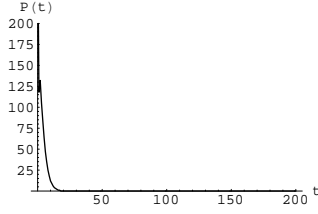
$$a_2 (P^\diamond)^2 + a_1 P^\diamond + a_0 = 0 \quad (33)$$

with

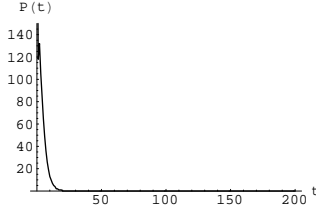
$$\begin{aligned} a_0 &= \mu_s \left(c_2 + \frac{1}{\tilde{\mathcal{R}}'} \bar{S} \right) - c_1 = \mu_s \bar{S} \left(\frac{1}{\tilde{\mathcal{R}}'} - 1 \right), \\ a_1 &= \frac{\xi}{\tilde{\mathcal{R}}'} \bar{S} \left(c_2 \frac{\bar{S}}{\tilde{\mathcal{R}}'} + 1 + \frac{\mu_s}{\mu_s + \delta_s} \right), \\ a_2 &= \frac{\xi^2}{\tilde{\mathcal{R}}'} \frac{\bar{S}}{\mu_s + \delta_s}. \end{aligned}$$

Obviously, $a_1 > 0$ and $a_2 > 0$. It is also clear that $a_0 > 0$ if $\tilde{\mathcal{R}}' < 1$ and $a_0 < 0$ if $\tilde{\mathcal{R}}' > 1$. It follows that equation (33) has a unique positive solution if $\tilde{\mathcal{R}}' > 1$ and no positive solution

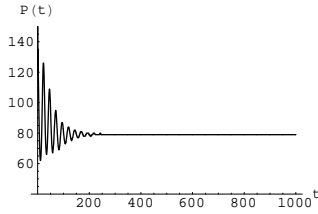
if $\tilde{\mathcal{R}}' \leq 1$. This finishes the proof of part (a). We do not have an analytic proof for part (b) but our numerical simulations show that a (Hopf) bifurcation occurs at a critical value of $\mathcal{R} \in (5, 6)$ or $c_1 \in (650, 700)$ (see Figure 2).



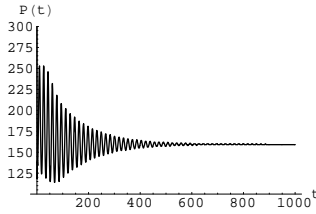
(a) $c_1 = 200, \mathcal{R}_0 = 0.5022$



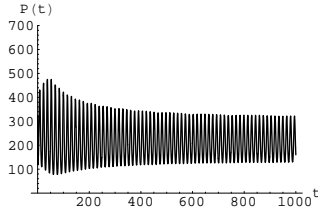
(b) $c_1 = 250, \mathcal{R}_0 = 0.8739$



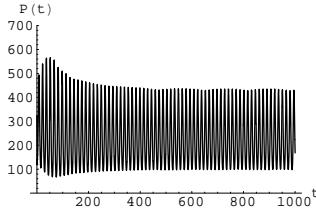
(c) $c_1 = 400, \mathcal{R}_0 = 2.7622$



(d) $c_1 = 600, \mathcal{R}_0 = 5.2734$



(e) $c_1 = 700, \mathcal{R}_0 = 6.5289$



(f) $c_1 = 800, \mathcal{R}_0 = 7.7845$

Figure 2: Plots of the number of adult parasites $P(t)$ vs. time for different values of c_1 or equivalently \mathcal{R} . In (a) and (b) $\mathcal{R} < 1$ and the parasite-free steady state is stable. In (c)–(f) $\mathcal{R} > 1$ and the parasite population either converges to a positive level or converges to a stable periodic solution suggesting that a Hopf bifurcation occurs for some value of $\mathcal{R} \in (5, 6)$.

4 An application to disease control

The analysis of the model presented in the previous sections suggests that the reproductive number \mathcal{R} is directly related to the disease prevalence and that reduction of \mathcal{R} will help control of the disease. A remarkable advantage of the age-structure in our model is that it

Table 2: Distribution of parameters used for the sensitivity/uncertainty analysis.

Parameter's meaning	Parameter	Distribution
$\beta(1) \sim \beta(10)$	β_1	in $(7.2 \times 10^{-5}, 8.8 \times 10^{-5})$, with peak 8.0×10^{-5}
$\beta(11) \sim \beta(20)$	β_2	in $(9.0 \times 10^{-5}, 1.1 \times 10^{-4})$, with peak 1.0×10^{-4}
$\beta(21) \sim \beta(30)$	β_3	in $(7.2 \times 10^{-5}, 8.8 \times 10^{-5})$, with peak 8.0×10^{-5}
$\sigma(1) \sim \sigma(10)$	σ_1	in $(0.27, 0.33)$, with peak 0.3
$\sigma(11) \sim \sigma(20)$	σ_2	in $(0.27, 0.33)$, with peak 0.3
$\sigma(21) \sim \sigma(30)$	σ_3	in $(0.27, 0.33)$, with peak 0.3
ξ	ξ	in $(0.0018, 0.0022)$, with peak 0.002

makes possible the design of age-targeted control strategies. In this section we first study how the variability of \mathcal{R} depends on the uncertainty in the estimation of parameters that determine \mathcal{R} . Then we explore how various age-dependent treatment programs may affect the disease severity (measured by the mean parasite load). Finally we look at the impact of changes in various parameters on the reduction of \mathcal{R} .

4.1 Sensitivity and uncertainty analysis

There are several parameters or parameter functions (dependent of age) involved in the model whose values are difficult to obtain. For example, the human-to-snail transmission rate ρ and the age dependent snail-to-man transmission rate $\beta(a)$. To study the impact of the uncertainty of these parameters on the variability of \mathcal{R} we use the Latin hypercube sampling (LHS) method which allows each of the input parameters to have a distribution in stead of a single value. According to [6, 15], schistosomiasis infection is highest among the age group 11–20. For ease of demonstration, we assume that the population of all ages can be divided into the following age groups: $a_{i-1} < a \leq a_i$ (group i) where $a_i = 10i$ (e.g., $a_0 = 0, a_1 = 10$, etc.), and $\beta(a)$ is a step function with $\beta(a) = \beta_i = \text{constant}$ for $a_{i-1} < a \leq a_i$. Similarly, $\sigma(a)$ is also assumed to be a step function with $\sigma(a) = \sigma_i = \text{constant}$ for $a_{i-1} < a \leq a_i$. That is

$$\beta(a) = \begin{cases} \beta_i & \text{if } a_{i-1} < a \leq a_i, \quad i = 1, 2, \dots, 7 \\ 0 & \text{if } a > 70, \end{cases} \quad (34)$$

$$\sigma(a) = \begin{cases} \sigma_i & \text{if } a_{i-1} < a \leq a_i, \quad i = 1, 2, \dots, 7 \\ 0 & \text{if } a > 70, \end{cases}$$

where β_i and σ_i are constants. Each of these parameters is assumed to have a distribution (see Table 2). Figure 3 shows histograms of the values obtained from LHS for β_1 and ξ (from a sample size of 1000). For the calculation of \mathcal{R} we have chosen values of other parameters (e.g., $\Lambda_h =, \mu_p =, \alpha =, \mu_s =, \delta_s =$) from [9]. The age-specific human natural death rate $\mu_h(a)$ is adopted from [13]. Histograms of the estimated \mathcal{R} value from LHS are shown in Figure 4. We observe that when there is no treatment the probability of \mathcal{R} being greater than one is 1 with mean=1.37 and variance=0.12 (see Table 3). Under the treatment program described in Table 2 the probability of \mathcal{R} being less than one is 0.76 with mean=0.91 and variance=0.08 (see Table 3).

Note: For Table 2 it is necessary to choose different $\beta(a)$ otherwise there is no age difference in any parameters—no point to age group analysis. Since β_2 is changed, the results for \mathcal{R} needs to be checked. Also the sensitivity to σ

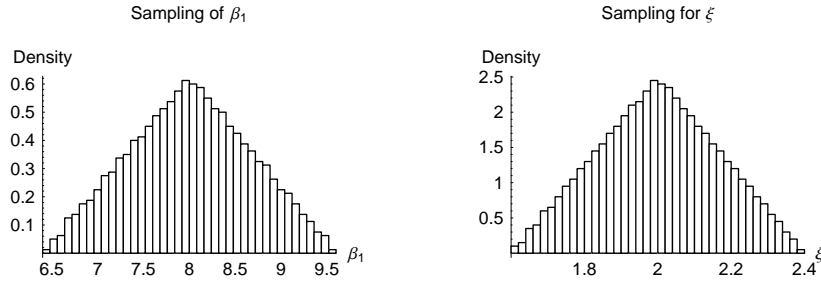


Figure 3: The histograms of the values obtained from Latin hypercube sampling for the input parameter variables (shown only for β_1 and ξ). The results are from one replication with a sample size of 1000. It is scaled to 10^{-5} for β_1 and to 10^{-3} for ξ .

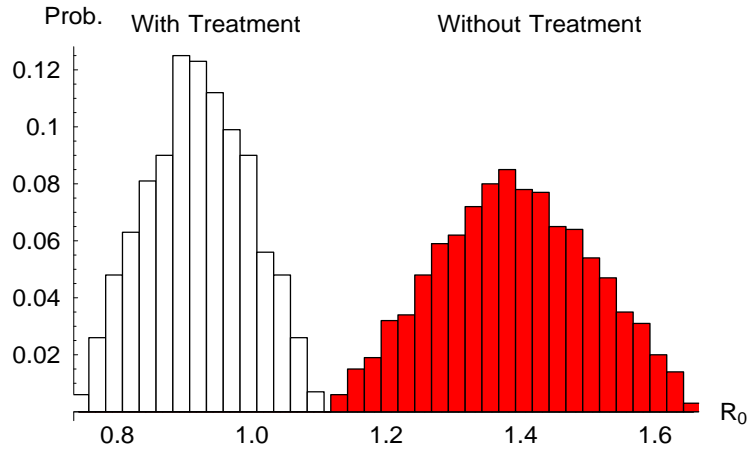


Figure 4: The histograms of \mathcal{R} from simulations in two cases. The unshaded graph on the left is for the case where there is a uniform treatment (e.g., $\sigma = 0.3$) and the shaded graph on the right is for the case when there is no treatment.

The independent effect of a single parameter on \mathcal{R} can be determined by looking at some of the statistics obtained from the sensitivity analysis such as the partial rank correlation coefficients (PRCCs) which are given in Table 4. The ordering of these PRCCs directly corresponds to the level of statistical influence on the variability of \mathcal{R} that the associated

Table 3: Estimates of \mathcal{R} from 10 Latin hypercube sampling replications

Replication no.	Without Treatment			With Treatment		
	Mean	Std Var	$P(\mathcal{R}_0 > 1)$	Mean	Std Var	$P(\mathcal{R}_0 > 1)$
1	1.3731127	0.1145590	1	0.9129636	0.0762348	0.137
2	1.3731073	0.1145244	1	0.9129563	0.0762316	0.136
3	1.3731040	0.1145516	1	0.9129585	0.0762391	0.136
4	1.3731086	0.1145362	1	0.9129704	0.0762368	0.137
5	1.3731028	0.1145132	1	0.9129612	0.0762321	0.137
6	1.3730981	0.1145554	1	0.9129714	0.0762351	0.137
7	1.3730886	0.1145143	1	0.9129703	0.0762509	0.137
8	1.3731106	0.1145575	1	0.9129565	0.0762246	0.136
9	1.3731069	0.1145316	1	0.9129614	0.0762440	0.137
10	1.3730897	0.1145101	1	0.9129673	0.0762381	0.137
Mean	1.3731029	0.1145353	1	0.9129637	0.0762367	0.1367
SE	8.34×10^{-6}	1.95×10^{-5}	0	5.83×10^{-6}	7.17×10^{-6}	0.000483

input parameter has due to its own estimation uncertainty. Since the PRCC value for σ_2 is negative and has largest absolute value it suggests that \mathcal{R} is more sensitive to the change in σ_2 . Hence, increasing the treatment efficacy for the age group $10 < a < 20$ is more effective in reducing \mathcal{R} and consequently reducing the disease severity.

Check σ_2 for Table 4...

We can also explore the effectiveness of various treatment programs in reducing \mathcal{R} be directly examining the formula for \mathcal{R} (i.e., without assuming distributions for input param-

Table 4: PRCCs for \mathcal{R} and the input parameter variables over 10 Latin hypercube sampling replications.

Input parameter	PRCC	p -value
β_1	0.67112	< 0.0001
β_2	0.69075	< 0.0001
β_3	0.63749	< 0.0001
σ_1	-0.11323	< 0.0001
σ_2	-0.43030	< 0.0001
σ_3	-0.17667	< 0.0001
ξ	0.97769	< 0.0001

eters). Consider the case of constant birth rate of snails. A formula for \mathcal{R} is given in (9) which can be rewritten as (by exchanging the order of integration and letting $a = w + u$)

$$\begin{aligned}\mathcal{R} &= \xi \frac{\Lambda_s}{\mu_s} \int_0^\infty \int_0^a \beta(w) \Lambda_h \pi(w) \mathcal{K} e^{-\int_w^a [\mu_h(s) + \mu_p + \alpha + \sigma(s)] ds} dw da \\ &= C \sum_{i=1}^8 I_i,\end{aligned}\tag{35}$$

where $C = \xi \frac{\Lambda_s}{\mu_s} \Lambda_h \mathcal{K}$ is a constant (independent of β and σ) and

$$I_i = \int_{a_{i-1}}^{a_i} \int_0^a \beta(w) e^{-\int_w^a [\mu_h(s) + \mu_p + \alpha + \sigma(s)] ds} dw da.$$

For simplicity we assume that the natural human death rate $\mu_h(a)$ is constant and that only σ values for the first three groups are changing. Using (34) for $\beta(a)$ and $\sigma(a)$ we can evaluate \mathcal{R} by evaluating each I_i . Notice that I_i depends on β_j and σ_j for all $j \leq i$. For example, denoting $\mu_h + \mu_p + \alpha$ by d we have

$$\begin{aligned}I_2 &= \int_{10}^{20} \int_0^a \beta(w) e^{-\int_w^a (d + \sigma(s)) ds} dw da \\ &= \int_0^{10} \int_0^a \beta_1 e^{-\int_w^a (d + \sigma_1) ds} dw da \\ &\quad + \int_{10}^{20} \left[\int_0^{10} \beta_1 e^{-\int_w^{10} (d + \sigma_1) ds - \int_{10}^a (d + \sigma_2) ds} dw + \int_{10}^a \beta_2 e^{-\int_w^a (d + \sigma_2) ds} dw \right] da \\ &= \frac{10\beta_1}{d + \sigma_1} + \frac{\beta_1 [e^{-10(d + \sigma_1)} - 1]}{(d + \sigma_1)^2} + \frac{\beta_1 [e^{-10(d + \sigma_1)} - 1] [e^{-10(d + \sigma_2)} - 1]}{(d + \sigma_1)(d + \sigma_2)} \\ &\quad + \frac{10\beta_2}{d + \sigma_2} + \frac{\beta_2 [e^{-10(d + \sigma_2)} - 1]}{(d + \sigma_2)^2}.\end{aligned}$$

To see the effect of each σ_i ($i = 1, 2, 3$) on the reduction of \mathcal{R} we look at the partial derivative of \mathcal{R} with respect to σ_i while keeping the other values of σ_j ($j \neq i$) fixed at the same constant (see Figure 5). A larger absolute value of $\frac{\partial \mathcal{R}}{\partial \sigma_i}$ indicates more effectiveness. Figure 5 shows that, for the chosen β_i values, σ_2 is more influential to \mathcal{R} than all other σ_j ($j \neq 2$). As the transmission rate is assumed to be highest in the age group $10 < a < 20$ (β_2 has the largest value), this suggests that treatment strategies should target the age group that has a higher infection rate.

4.2 Age-targeted control strategies

The above sensitivity analysis of \mathcal{R} suggests that a control program will be more effective when more treatment effort is given to the age group with the higher infection rate—as

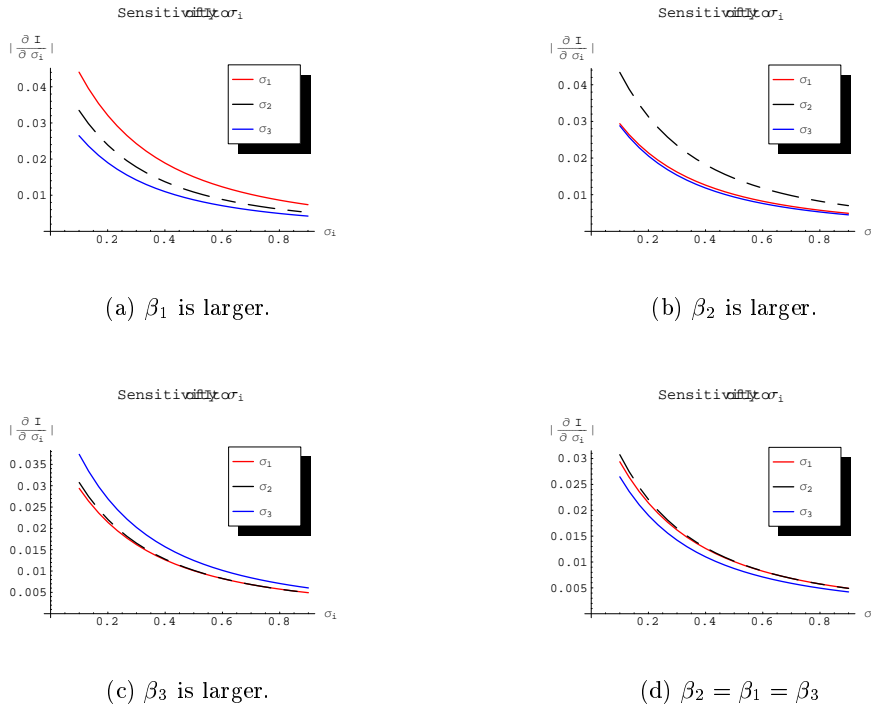
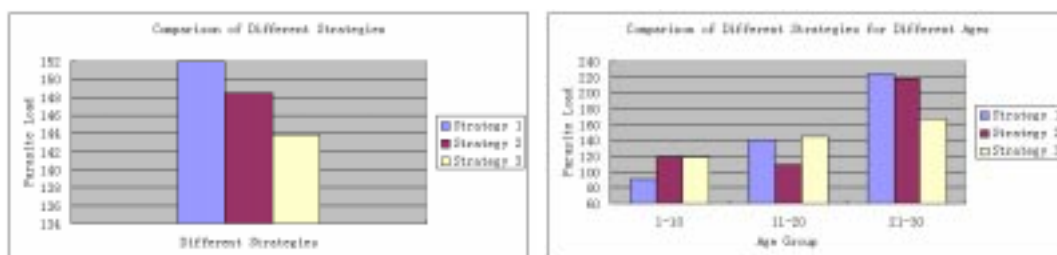


Figure 5: Plots of $\left| \frac{\partial I}{\partial \sigma_i} \right|$ vs σ_i ($i = 1, 2, 3$). The curve for σ_i is obtained by choosing $\sigma_j = 0.3$ for $j \neq i$. It shows that changing the treatment rate of the age group that has the highest infection rate always has the largest impact on I or equivalently on \mathcal{R} .

intuition suggests. We now compare this result with efficacy measures obtained by looking at the mean parasite load within humans under different control programs. For illustration purposes we use the same $\beta(a)$ function given in (34), and consider control strategies with various age-targeted treatment programs. Assume that a baseline treatment program is to treat all age groups at the same rate $\sigma = 0.2$ (σ is determined by the frequency of treatment and the coverage of the population). First, we consider the scenario in which only one age group will be given a treatment rate twice as higher ($\sigma = 0.4$) while all other age groups have the same treatment rate (see Table 5. Only three strategies are discussed). The criterion we use in this paper to assess the effectiveness of a control program is the mean parasite load (the ratio of the total number of parasites to the total number of humans) denoted by M_k for Strategy k . We also look at the mean parasite load within each age group denoted by m_{ki} where the index i stands for the i -th age group). We numerically integrate the system (5) for a given set of parameters. After the system has stabilized we calculate the mean parasite load. Figure 6 shows the outcomes of the three strategies. Figure 6(a) shows that the strategy that targets the age group $11 \leq a \leq 20$ is the most effective one as it results in a lowest overall mean parasite load while the strategy that targets the age group $0 \leq a \leq 10$ is the least effective one. More detailed age-dependent distributions of the parasite load corresponding to these treatment programs are given in Figure 6(b), which shows that the strategy II will results in a more uniform parasite distribution among all age groups.

Table 5: Treatment programs targeted at a single age group.

	Treatment value $\sigma(\cdot)$		
	Age 0-10	Age 11-20	Age 21-30
Strategy 1	0.4	0.2	0.2
Strategy 2	0.2	0.4	0.2
Strategy 3	0.2	0.2	0.4



(a) Overall mean parasite load.

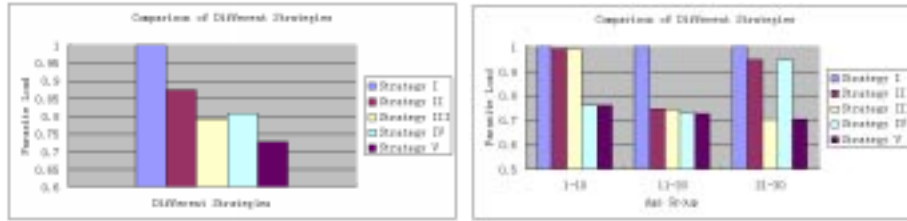
(b) Age-dependent parasite load.

Figure 6: Comparison of treatment strategies I, II and III for the case when the infection rate is higher in the age group $11 \leq a \leq 20$.

In Figure 7 we compare treatment programs that target one, two, or three age groups, i.e., these targeted groups will have a higher treatment rate while all other groups have the same baseline treatment rate $\sigma = 0.2$ (see Table 6). The effect of each program is assessed using the reduction in the parasite load of a program relative to the baseline treatment program (Strategy I), i.e., the ratio m_{ki}/m_{1i} or M_k/M_1 ($k = 2, 3, \dots, 5, i = 1, 2, \dots, 5$). These ratios are plotted in Figure 7. Figure 7(a) shows that Strategy II, which targets the single age group $10 < a \leq 20$, can further reduce the mean parasite load by about 13% of the mean load resulted from the baseline treatment ($M_2/M_1 \approx 0.87$). When the treatment coverage is doubled (increasing the treatment rate in two age groups, e.g., Strategies III and IV) the reduction in the mean load is an additional 7% ($M_k/M_1 \approx 0.80$ for $k = 3, 4$), and when the treatment coverage is tripled (increasing the treatment rate in three age groups, e.g., Strategies V) the mean parasite load is reduction by another 7% ($M_5/M_1 \approx 0.73$). This type of information is especially useful if the cost associated with the treatment program is also a factor. Figure 7(b) shows the distribution of the mean parasite load among age groups under the five treatment strategies.

Table 6: Treatment programs targeted at one, two or three age groups.

	Treatment value $\sigma(\cdot)$		
	Age 0-10	Age 11-20	Age 21-30
Strategy I	0.2	0.2	0.2
Strategy II	0.2	0.4	0.2
Strategy III	0.2	0.4	0.4
Strategy IV	0.4	0.4	0.2
Strategy V	0.4	0.4	0.4



(a) Mean parasite load over all ages.

(b) Mean parasite load in age groups.

Figure 7: Plots of the relative mean parasite load M_k/M_1 ($k = 2, 3, \dots, 5$) and the age-dependent relative mean parasite load m_{ki}/m_{1i} ($k = 2, 3, \dots, 5$, $i = 1, 2, \dots, 5$) under the five treatment strategies listed in Table 6.

5 Discussion

In this paper we studied an integral differential equation model that describes the disease transmission of schistosomiasis. Partial differential equations are used because of the age structures of both human hosts and snail hosts. The age structure of human hosts is needed to incorporate the fact that the infection rate of human hosts is quite dependent on the age of the host, and the infection-age structure of snail hosts is needed because of the fact that the cercaria releasing rate of infected snails is dependent of the infection age of the snail. Mathematical properties of the model are analyzed in terms of existence and stability of possible steady states. The reproductive number \mathcal{R} is calculated and shown to determine the stability of the steady states. We considered two cases for the snail birth rate: 1) constant birth rate $b_1(S, I)$ and 2) density-dependent birth rate $b_2(S, I) = c_1 S / (c_2 + S + I)$. For both cases we proved that the disease-free steady state E_0 is globally asymptotically stable if $\mathcal{R} < 1$ (Case 1) or $\mathcal{R}' < 1$ (Case 2) and it is unstable if $\mathcal{R} > 1$ or $\mathcal{R}' > 1$. For Case 1 we proved that when $\mathcal{R} > 1$ an unique endemic steady state E^* exists and is locally asymptotically stable. The stability of E^* is proved analytically only for the case when $\alpha = 0$ and is extended to the case of $\alpha > 0$ numerically. For Case 2 we have an analytic proof only for the existence of an unique endemic steady state E^\diamond and its stability is studied numerically. The numerical simulations show that E^\diamond may lose its stability and stable periodic solutions develop via a Hopf bifurcation at some critical value of a model parameter.

We then studied the effect of various age-dependent treatment strategies on the disease control for the case of $b_1(S, I) = \Lambda_s$ using two approaches. The first approach is to study the sensitivity of \mathcal{R} to changes in the age-specific treatment rate, and the second approach is to consider the reduction in the mean parasite load within human hosts. Both approaches seem to suggest that control strategies that target the age group with a higher infection rate is the most effective strategy. We have not considered the cost factor that may be associated with a given age-dependent control program or the possible development of parasite resistance to chemotherapy. The consideration of drug resistance will lead to a model with multiple parasite strains (see [8] for a model without age-structure).

Although the introduction of an age-structure of human hosts makes the model much more difficult to analyze, it provides an important advantage for the study of age-dependent control strategies, especially given that the human infection rate is highly age-dependent. In this paper we have only considered a simple age-structure, i.e., the age-dependent infection rate $\beta(a)$ and treatment rate $\sigma(a)$ have been assumed to be step functions over several age groups. More insights may be obtained if these assumptions can be relaxed. Nevertheless, the results in this paper may provide some theoretical guidance for designing age targeted control strategies.

References

- [1] Araujo, N. *et al.* (1980). Susceptibility to chemotherapeutic agents of strains of schistosoma mansoni isolated from treated and untreated patients., *Am. J. Trop. Med. Hyg.* 29, 890.

- [2] Anderson, R. M. and May, R. M. (1978). Regulation and stability of host-parasite population interactions. I. Regulatory processes, *J. Animal Ecology* 47, 219-247.
- [3] Anderson, R. M. and May, R. M. (1979). Prevalence of schistosome infections within molluscan populations: observed patterns and theoretical predictions, *Parasitology* 79, 63-94.
- [4] Castillo-Chavez, C. and Feng, Z. (1998). Global stability of an age-structure model for TB and its applications to optimal vaccination strategies, *Mathematical Biosciences* 151, 135-154.
- [5] Chan, M. S. *et al.* (1995). The development of an age structured model for schistosomiasis transmission dynamics and control and its validation for *Schistosoma mansoni* , *Epidemiol. Infect.* 115, 325-344.
- [6] Cristiano L.M. and Sergio V.P. (2004). Factors associated with Schistosomia mansoni in a population from the municipality of Jaboticatubas, State of Minas Gerais, Brazil, *Mem. Inst. Oswaldo Cruz, Rio de Janeiro* 99, 127-134.
- [7] Dobson, A. P. (1988). The population biology of parasite-induced changes in host behavior, *The Quarterly Review of Biology* 63, 139-165.
- [8] Feng, Z., Curtis, J. and Minchella, and D. J. (2001). The influence of drug treatment on the maintenance of schistosome genetic diversity, *J. Math. Bio.* 43, 52-68.
- [9] Feng, Z., Li, C-C., and Milner, F. A. (2002). Schistosomiasis models with density dependence and age of infection in snail dynamics, *Mathematical Biosciences* 177-178, 271-286.
- [10] Feng, Z., Eppert, A., Milner, F. A., Minchella, D. J. (2004). Estimation of Parameters Governing the Transimission Dynamics of Schistosomes, *Applied Mathematics Letters* 17, 1105-1112.
- [11] Gripenberg, S.-O. Londen, O. Staffans. (1990) Volterra integral and functional equations, Cambridge University, Cambridge.
- [12] May, R. M. and Anderson, R. M. (1979). Population biology of infectious diseases II, *Nature* 280, 455-461.
- [13] Hoyert, D.L., Kuang, H-C, and Smith, B.L. (2005) Deaths: Preliminary Data for 2003., *National Vital Statistics Reports* 53(15),
- [14] Savioli, L. and Blower, S. (1990). Uncertainty and sensitivity analysis of the basic reproductive rate: Tuberculosis as an example, *American J. of Epidemiology* 145(12), 1127-1138.
- [15] Sturrock RF (2001). Schistosomiasis epidemiology and control: How did we get here and where should be go?, *Mem. Inst. Oswaldo Cruz, Rio de Janeiro* 96, Suppl., 17-27.
- [16] Thieme, H. R. (1993). Persistence under relaxed point-disspativity (with application to an endemic model), *SIAM J. Math. Anal.* 24(2), 407-435.

- [17] Woolhouse, M. E. J. (1991). On the application of mathematical models of schistosome transmission, *Acta Tropica* 49, 241.
- [18] Xu, D., Curtis, J., Feng, Z., and Minchella, D.J. (2005). On the role of schistosome mating structure in the maintenance of drug resistant strains, *Bulletin of Mathematical Biology* 67 (6), 1207-1226.